Journal of Power Sources 246 (2014) 95–102

Contents lists available at ScienceDirect

Journal of Power Sources

journal homepage: www.elsevier.com/locate/jpowsour

# Enhanced electrochemical properties of $TiO_2$(B) nanoribbons using the styrene butadiene rubber and sodium carboxyl methyl cellulose water binder

Xiao Yan [a], Yongquan Zhang [a], Kai Zhu [a], Yu Gao [a], Dong Zhang [a], Gang Chen [a,b], Chunzhong Wang [a,b], Yingjin Wei [a,*]

[a] Key Laboratory of Physics and Technology for Advanced Batteries, Ministry of Education, College of Physics, Jilin University, Changchun 130012, PR China
[b] State Key Laboratory of Superhard Materials, Jilin University, Changchun 130012, PR China

## HIGHLIGHTS

- $TiO_2$(B) nanoribbons were prepared by freeze-drying assisted hydrothermal process.
- SBR/CMC water binder was first used to prepare $TiO_2$(B) anode electrode.
- Excellent capacity retention and rate performance were obtained using SBR/CMC.
- SBR/CMC is more promising than PVDF for preparation of $TiO_2$(B) anode electrode.

## GRAPHICAL ABSTRACT

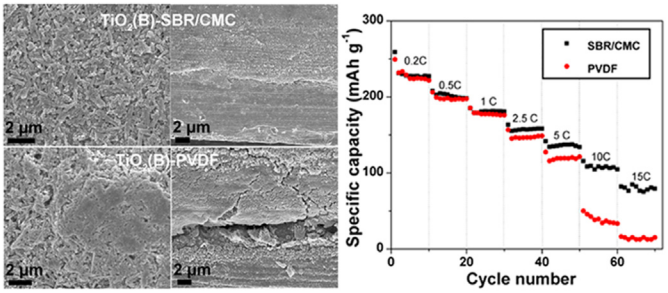


## ARTICLE INFO

*Article history:*
Received 31 May 2013
Received in revised form
15 July 2013
Accepted 16 July 2013
Available online 26 July 2013

*Keywords:*
Lithium-ion battery
Titanium dioxide
Binder
Styrene butadiene rubber
Carboxyl methyl cellulose

## ABSTRACT

$TiO_2$(B) anode for lithium-ion batteries is prepared by the hydrothermal method. The styrene butadiene rubber and sodium carboxyl methyl cellulose (SBR/CMC) and polyvinylidene fluoride (PVDF) binders are used to prepare the $TiO_2$(B) electrodes. Scanning electron microscope and electrochemical impedance spectroscopy show that the electrode prepared with SBR/CMC has better electrode maintainability and electrochemical kinetics which result in better electrochemical performance. The optimized SBR/CMC binder content is proposed to be in the range of 12–15 wt%. In addition, the 1 M $LiPF_6$ electrolyte dissolved in EC:DMC = 3:7 is more suitable for the $TiO_2$(B) electrode. Using this suggested binder content and electrolyte, the $TiO_2$(B) material exhibits superior capacity retention and rate capability. Even at the 10 C rate, the material still shows a discharge capacity of 142.5 mAh $g^{-1}$ which keeps very well after 800 cycles. Based on this work, it is concluded that SBR/CMC is a promising binder for the $TiO_2$(B) anode which provides not only better electrochemical performance but also more cheaper and environmental friendly than PVDF.



## 1. Introduction

Lithium-ion batteries have become leading candidates for energy storage due to their high energy/power densities, low toxicity and long cycle life. They are widely applied in cell phones, laptop computers and other electronic devices, and are also attractive for plug-in-hybrid electric vehicles and electric vehicles. Currently,

* Corresponding author. Tel./fax: +86 431 85155126.
*E-mail address:* yjwei@jlu.edu.cn (Y. Wei).

0378-7753/$ – see front matter © 2013 Elsevier B.V. All rights reserved.
http://dx.doi.org/10.1016/j.jpowsour.2013.07.072

graphite and other carbonaceous materials are the most commonly used anode materials in lithium-ion batteries. However, they suffer from a rather high irreversible capacity during the initial cycles and serious safety problems during repeated charge–discharge cycling. In recent years, titanium dioxides ($TiO_2$) including anatase [1–3], rutile [4,5] and $TiO_2$(B) [6–10] have attracted great interest as anode materials for lithium-ion batteries. The higher voltage of titanium dioxides (~1.6 V vs. $Li/Li^+$) endows them with greater overcharge protection than graphite. Also the material can be made in nanostructured forms thus permitting access to fast charge–discharge rates. A major problem for the $TiO_2$ anodes is their high working voltages that compromising the cell voltage and hence energy storage. But this can be partly overcome by using higher voltage cathodes such as $LiNi_{0.5}Mn_{1.5}O_4$.

Among different titanium dioxide anodes under investigation, $TiO_2$(B) is the most attractive one in terms of its large specific capacity and excellent rate capability. The edge- and corner- shared $TiO_6$ octahedra of $TiO_2$(B) construct a more opened structure than rutile and antase, which is favorable for $Li^+$ ion storage and transportation. For example, $TiO_2$(B) can store 240 mAh $g^{-1}$ in its bulk form, and this increases to about 330 mAh $g^{-1}$ by preparation of nanostructured forms [11]. In contrast, the practical capacities for the anatase and rutile phases are limited to 168 mAh $g^{-1}$ [12–18]. On the other hand, it has been identified that the $Li^+$ ion intercalation into $TiO_2$(B) is a pseudocapacitive faradic process, rather different from the solid-state diffusion process for anatase, thus easily to obtain excellent performance at higher charge–discharge rates [9,19].

In order to enhance the electrochemical performance of lithium-ion batteries, researchers are not only trying to create new electrode materials, but also searching for new electrode processing techniques. Binder is an important component for battery electrodes whose major function is to act as an effective dispersion agent to connect the electrode species together and then steadily adhere them to the current collectors. The most commonly used binder in commercial lithium-ion batteries is poly(vinylidene) fluoride, PVDF, due to its high electrochemical stability and good connection between the electrode materials and current collectors. However, PVDF is always dissolved into some organic solvents such as *N*-methy-l-2-pyrrolidone (NMP). It is known NMP is a volatile and combustible solvent which causes safety problems and severe pollution. In addition, strict control of humidity (less than 2%) is needed during the electrode manufacturing process.

In the last few years, combination of sodium carboxyl methyl cellulose (CMC) and styrene butadiene rubber (SBR) has attracted great attention as a new binder for lithium-ion batteries. CMC is a typical polymeric derivative of cellulose which contains carboxylate anion and hydroxyl functional groups. The existing of these two groups makes CMC a water-soluble binder and an effective thickening agent. SBR as an elastomer has higher flexibility, stronger binding force and better heat resistance than PVDF. In addition, it is very attractive that the price of CMC is about 1–2 EUR $kg^{-1}$ and SBR is about 0.2–1 EUR $kg^{-1}$, which are much cheaper than that of PVDF (15–18 EUR $kg^{-1}$) [20]. SBR/CMC binder has been used in some anode materials including graphite [21], transition metal oxides [22,23] and silicon based materials [24,25] which have been demonstrated with enhanced electrochemical performance. More recently, CMC or SBR/CMC binder has been applied to prepare anatase anode by different groups [26–28]. It is showed that the use of this water binder can provide better capacity retention and higher rate capability than PVDF does. However, to the best of our knowledge there is no attempt to prepare $TiO_2$(B) electrode using the SBR/CMC binder. Herein in this work, we synthesized $TiO_2$(B) nanoribbons using the hydrothermal method. Then we prepared $TiO_2$(B) electrode using the SBR/CMC binder. This new electrode showed improved electrochemical properties compared with the traditional PVDF-based $TiO_2$(B) electrode. Further, in order to optimize the battery performance, we studied the electrochemical properties of the $TiO_2$(B) electrode in different electrolytes and with different binder contents.

## 2. Experimental

### 2.1. Sample preparation

$TiO_2$(B) nanoribbons was synthesized by the hydrothermal process followed by freeze-drying post treatments. As a typical synthesis procedure: 0.4 g of $TiO_2$ (P25, Degussa) was dispersed in NaOH solution (40 mL, 10 M). After ultrasonic treatment for 30 min and stirring for another 30 min, the resulting suspension was transferred into a 50 ml autoclave. The autoclave was then sealed and heat treated at 180 °C for 72 h. After cooling down to room temperature, the obtained white precipitates were isolated from the solution by centrifugation and subsequently acid washing, followed by constant stirring in 0.1 M of HCl solution for 4 h. The obtained proton exchanged titanate precipitate was then centrifuged, and washed with deionized water for three times. The material was frozen at −30 °C for 2 h and then freeze-drying the ice solid product under vacuum for 20 h. At last, the $TiO_2$(B) nanoribbons were prepared by heating the proton exchanged titanate precipitate at 400 °C for 4 h in air.

### 2.2. Material characterizations

Powder X-ray diffraction (XRD) of the $TiO_2$(B) nanoribbons was measured on a Bruker AXS D8 X-ray diffractometer with Cu Kα radiation ($\lambda$ = 1.54056 Å). Raman scattering of the product was performed on a Bruker FT-Raman using Nd-line laser source ($\lambda$ = 1064 nm). The morphology of the $TiO_2$(B) nanoribbons and the electrodes prepared with different binders were observed by scanning electron microscope (SEM, JEOL JSM-6700F). The microstructure of the $TiO_2$(B) nanoribbons was characterized by high resolution transmission electron microscope equipped with selected area electron diffraction (TEM/HRTEM/SAED, FEI Tecnai G2, 200 kV). The electronic conductivity of the electrode was measured by the four-point probe method.

### 2.3. Electrochemical measurements

Electrochemical studies of the $TiO_2$(B) nanoribbons were performed using 2032 coin cells with a metallic lithium foil as the counter electrode. Two different binders, SBR/CMC (SBR:CMC = 1:1 by w/w ratio) and PVDF were used for the preparation of electrodes. The SBR/CMC binder was dissolved in water and the PVDF binder was dissolved in NMP solvent. The electrodes were prepared by mixing 70 wt% of active material, 15 wt% of super P conductive additive and 15 wt% of PVDF (or SBR/CMC) binder, which was pasted onto a copper current collector. Hereafter the electrodes were denoted as $TiO_2$(B)–PVDF and $TiO_2$(B)–SBR/CMC correspondingly. Each electrode was 0.64 $cm^2$ in size and contained 1–2 mg of active material. The working and counter electrodes were separated by Celgard 2400 membrane. The electrolyte was a 1 M $LiPF_6$ dissolved in ethylene carbonate (EC) and dimethyl carbonate (DMC) (EC:DMC = 1:1, by v/v ratio). The batteries were assembled in an argon-filled glovebox with $H_2O$ and $O_2$ concentrations below 1 ppm. Galvonostatic charge–discharge was measured on a LAND (Wuhan, China) automatic battery tester. Cyclic voltammetry (CV) and electrochemical impedance spectroscopy (EIS) were performed on a VSP multichannel potentiostatic-galvanostatic system (Bio-Logic SAS, France). The EIS measurement was carried out using the

three-electrode cell in which a lithium foil and a lithium wire served as the counter and reference electrodes, respectively. The impedance spectra were recorded by applying an ac voltage of 5 mV in the frequency range from 200 kHz to 10 mHz.

## 3. Results and discussion

### 3.1. Structure and morphology of the $TiO_2$(B) nanoribbons

Crystallographic structure of the hydrothermally synthesized sample is examined by powder X-ray diffraction. The XRD pattern shown in Fig. 1 exhibits all the elaborate diffraction peaks of $TiO_2$(B) that having a monoclinic structure with the space group of C2/m. The framework of the $TiO_2$(B) structure is constructed from corrugated sheets of edge- and corner-sharing $TiO_6$ octahedra that are linked by bridging oxygen atoms to form a three-dimensional network [29]. This structure is more open than those of rutile and anatase, consequently making the material an effective host for lithium ion storage. The lattice parameters of the as-prepared $TiO_2$(B) product are calculated to be $a$ = 12.302 Å, $b$ = 3.754 Å, $c$ = 6.453 Å and $\beta$ = 106.401°, which are consistent with those recorded in JCPDS No. 74-1940. In addition, all the peaks in the diffraction pattern are broadened indicating that the $TiO_2$(B) product is a nano-sized material as we expected.

Further, the phase purity and short-range local structure of the $TiO_2$(B) product is studied by Raman scattering as shown in Fig. 2. The Raman pattern matches well with that of bulk $TiO_2$(B) powders except a weak peak located at 514.2 $cm^{-1}$ which is attributed to anatase $TiO_2$ [9]. This impurity phase is not easy to distinguish from X-ray diffraction because the major diffraction peaks of $TiO_2$(B) and anatase are overlapped, especially for nanocrystalline materials with broad diffraction peaks. From the relative intensity of the additional 514.2 $cm^{-1}$ Raman peak we think that the amount of anatase in the product should be very small. This impurity phase could be originated from the un-reacted anatase raw material or the partial transformation of $TiO_2$(B) to anatase that occurs during heat treatment, which is similar to that noted in previous reports [7,30].

The SEM images of the $TiO_2$(B) product under low and high magnifications are shown in Fig. 3a and b. It is seen that the sample has a large number of uniform nanoribbons which have a highly oriented growth behavior and a high aspect ratio with 50–200 nm in width and several micrometers in length. Thanks to the freeze-drying post treatments, the sample shows very good dispersion without significant agglomeration and twine. These features are conducive to electrode active materials in touch with electrolyte more effectively thus leading to satisfying battery performance. The ribbon-like morphology of the $TiO_2$(B) sample is further conformed by TEM as shown in Fig. 3c. Most part of the nanoribbons is uniformly distributed. But there are still some dense spots appearing on the nanoribbons. These dense spots could be due to the anatase nano particles but at present we are not able to confirm this speculation. Fig. 3d gives a typical high resolution transmission electron microscope (HRTEM) image and the corresponding selected area electron diffraction (SAED) pattern of a single $TiO_2$(B) nanoribbon. The two sets of lattice fringes with spaces of 0.595 nm and 0.362 nm can be attribute to the (200) and (110) planes of $TiO_2$(B). Combined with the HRTEM image and SAED pattern, it is believed that the $TiO_2$(B) nanoribbons are highly crystallized and grow along the [110] direction.

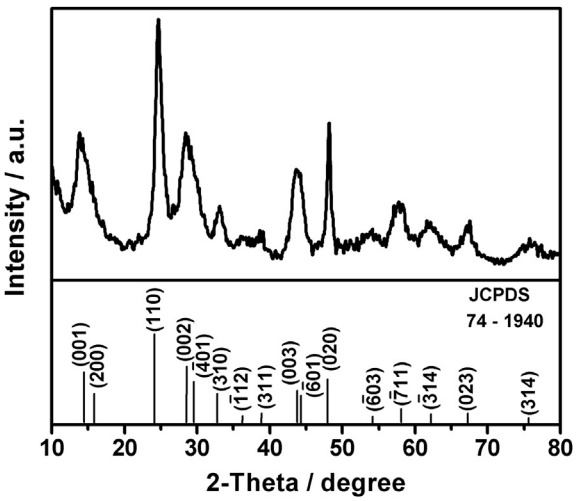


**Fig. 1.** XRD pattern of the $TiO_2$(B) nanoribbons.

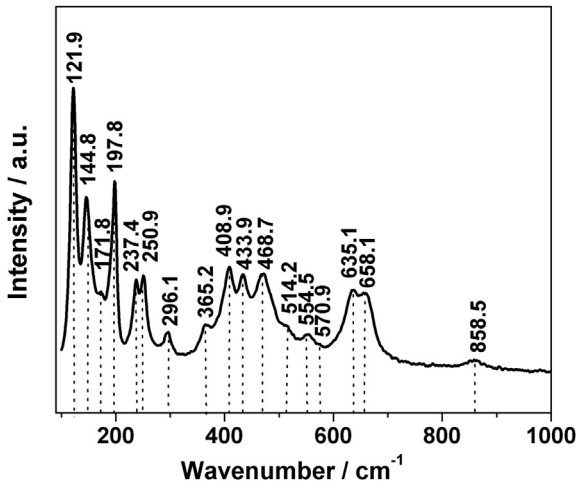


**Fig. 2.** Raman spectrum of the $TiO_2$(B) nanoribbons.

### 3.2. Morphologies of the electrodes

The morphologies of the $TiO_2$(B)–SBR/CMC and $TiO_2$(B)–PVDF electrodes before/after charge–discharge cycling are investigated by SEM. Fig. 4a and c compares the SEM images of the fresh electrodes prepared with different binders. From the first sight, the surface of $TiO_2$(B)–SBR/CMC is very flat and have a lot of small pores, while the $TiO_2$(B)–PVDF electrode has a rough surface and seems less compact than $TiO_2$(B)–SBR/CMC. A deep insight into the microstructures of the electrodes is obtained under a higher magnification as shown in the inset of SEM. Both electrodes show homogenous distribution of the $TiO_2$(B) active materials. But, the dispersion of super P carbon (small clusters under SEM) in the $TiO_2$(B)–PVDF electrode is much poorer than that in $TiO_2$(B)–SBR/CMC. More importantly, it is clear to see that the $TiO_2$(B) nanoribbons in the $TiO_2$(B)–SBR/CMC electrode are covered by a thin layer which is absent for $TiO_2$(B)–PVDF. This indicates that the SBR/CMC binder trends to form a thin polymer layer on the surface of the $TiO_2$(B) nanoribbons. In the $TiO_2$(B)–SBR/CMC electrode, this polymer layer would help to construct a highly effective three-dimensional network by bridging of the $TiO_2$(B) nanoribbons and uniform adsorption of the super P clusters. The morphology features of the $TiO_2$(B)–SBR/CMC electrode can help to form an efficient conductive network which is important for the electrochemical performance. By comparing the electric resistance of the $TiO_2$(B)–PVDF and $TiO_2$(B)–SBR/CMC electrodes, it is shown that the electrode using the SBR/CMC binder has smaller electric

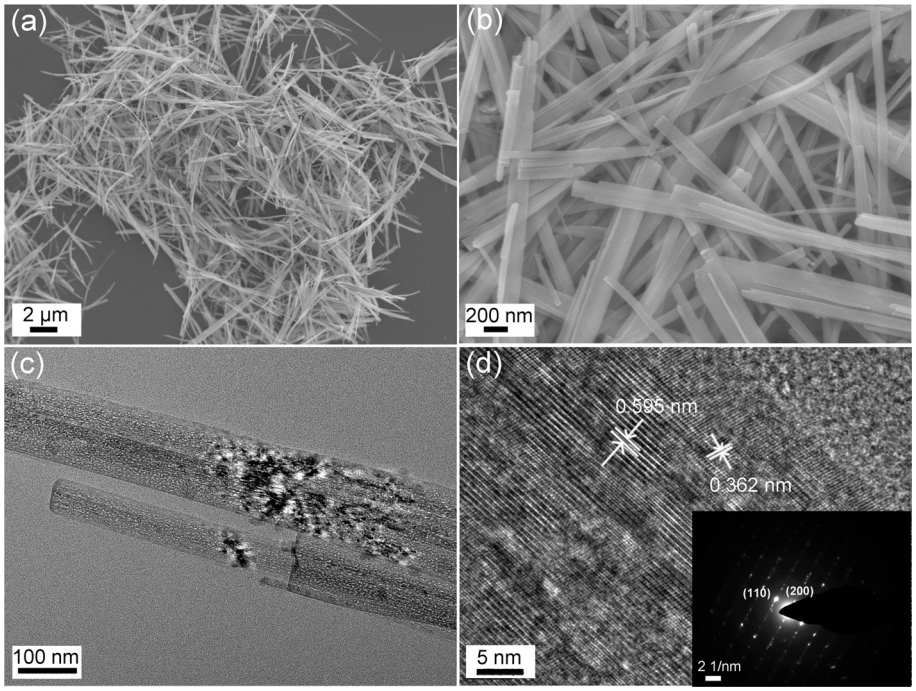


**Fig. 3.** (a) Low-magnification and (b) high-magnification SEM images of the $TiO_2$(B) nanoribbons, (c) TEM and (d) HRTEM images of the $TiO_2$(B) nanoribbons. Inset in (d) shows the corresponding SAED pattern.

resistance (2.03 Ω) than that prepared using the PVDF binder (30.02 Ω). In the battery system, small electrode resistance is critical for obtaining good capacity retention and high rate capability.

Then, galvanostatic charge–discharge is performed on the two electrodes in the voltage window of 1.0–3.0 V. Fig. 4b and d shows the SEM images of the $TiO_2$(B)–SBR/CMC and $TiO_2$(B)–PVDF electrodes after 50 cycles. In order to eliminate the effect of absorbent electrolyte, the electrodes have been completely washed off by dimethyl carbonate (DMC) before SEM measurement. Obviously, the $TiO_2$(B)–PVDF electrode undergoes severe changes after charge–discharge cycles. The whole electrode, not only the electrode surface but also the $TiO_2$(B) active material, is now covered by a thick gel film. According to H. Buqa et al. more and more PVDF binder will dissolve in the nonaqueous electrolytes with charge–discharge cycling. This leads to the gelation of PVDF and electrolyte which then continuously covers on the electrode [24]. In lithium-ion batteries too thick of such a gel film will block the $Li^+$ ions exchange, isolate the electrons transportation, and thus degrade the battery performance. In contrast to $TiO_2$(B)–PVDF, the $TiO_2$(B)–SBR/CMC electrode does not change much after 50 cycles. Even

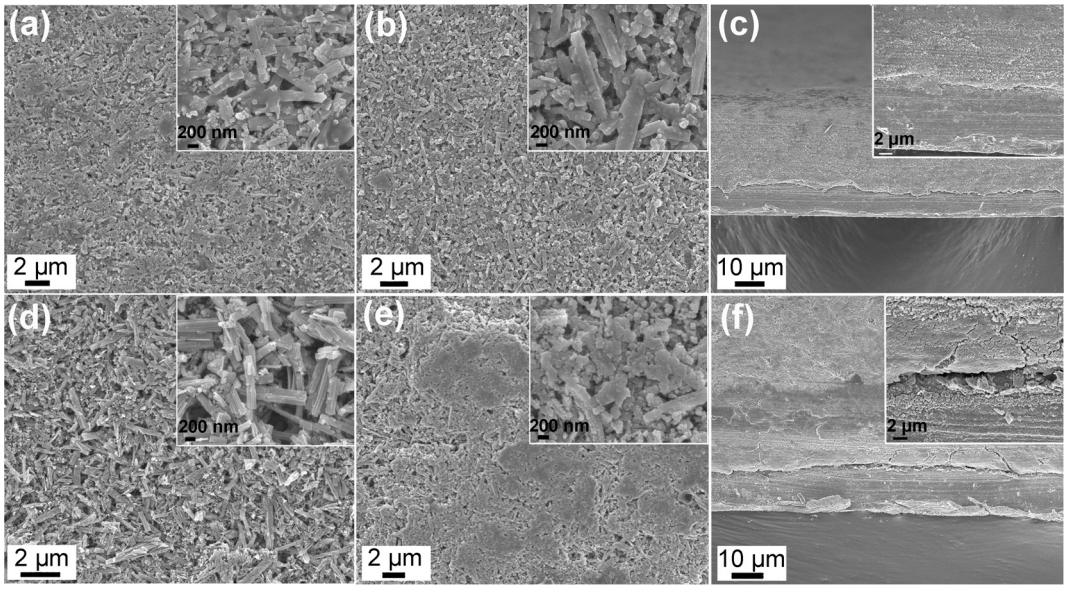


**Fig. 4.** SEM images of the $TiO_2$(B)–SBR/CMC (up) and $TiO_2$(B)–PVDF (down) electrodes, (a, d) the as-prepared electrodes, (b, e) the electrodes after 50 cycles, (c. f) cross-sections of the electrodes after 50 cycles.

though the surface layer on the $TiO_2$(B) nanoribbons becomes a little thicker with respect to the fresh electrode. The whole electrode is still very uniform and keeps a high porosity.

Fig. 4c and f presents the cross-section images of the cycled electrodes. It is seen that the electrode film on $TiO_2$(B)–SBR/CMC still remains good adherence to the current collector. While a big gap is found for $TiO_2$(B)–PVDF between the electrode film and the current collector. In addition, cracks are clearly visible in the $TiO_2$(B)–PVDF electrode. It is known that CMC is extremely stiff and brittle which easily to form cracks or slide off the current collector when used alone as the binder. Addition of SBR to CMC results in electrodes that are less brittle and, compared to PVDF, shows a smaller Yong's modulus, a larger maximum elongation and stronger adhesion strength to the current collector [31]. Due to these advantageous, the $TiO_2$(B) electrode prepared with SBR/CMC binder has better maintainability than that prepared with PVDF, which leads to its good electrochemical performance as will be shown below.

### 3.3. Electrochemical characterizations

Fig. 5 compares the CV curves of the $TiO_2$(B)–SBR/CMC and $TiO_2$(B)–PVDF electrodes at different scan rates in the voltage range of 1.0–3.0 V. Three cathodic peaks can be seen for the $TiO_2$(B)–SBR/CMC electrode at the scan rate of 0.1 mV $s^{-1}$ which are consistent with previous reports on $TiO_2$(B) anode [6,7,9,32]. The peak located at ~1.68 V (denoted as A peak) is a typical behavior for the lithium intercalation in anatase. The two peaks located around 1.48 V and 1.51 V (denoted as S1 and S2 peak) are due to the lithium intercalation in $TiO_2$(B). The $TiO_2$(B)–PVDF electrode shows a similar CV curve at the same scan rate. But, the A, S1 and S2 current peaks appear at 1.45 V, 1.19 V and 1.23 V, respectively. All of these voltages are lower than those observed for $TiO_2$(B)–SBR/CMC which indicates sluggish electrochemical kinetics of the $TiO_2$(B)–PVDF electrode. When increasing the scan rate, the $TiO_2$(B)–SBR/CMC electrode maintains a symmetrical CV curve, whereas the shapes of the cathodic and anodic peaks change greatly for the $TiO_2$(B)–PVDF electrode. We cannot even see the current peaks clearly when the scan rate reaches 1.0 mV $s^{-1}$. Well-shaped CV curves for the $TiO_2$(B)–SBR/CMC electrode indicates its good electrochemical reversibility and rate capability.

The charge–discharge cycling performance of different $TiO_2$(B) electrodes is studied in the voltage window of 1.0–3.0 V with the 0.2 C rate (1 C = 300 mA $g^{-1}$). Fig. 6a displays the voltage curves of the $TiO_2$(B)–PVDF and $TiO_2$(B)–SBR/CMC electrodes in the 1st, 5th and 50th cycles. Both electrodes display a pair of smooth slopes between 1.3 V and 1.8 V, which is different from the characteristic charge–discharge plateaus at ~1.7 V for anatase $TiO_2$. This is due to the different $Li^+$ ion intercalation mechanisms between $TiO_2$(B) and anatase. It has been identified that the $Li^+$ ion intercalation into $TiO_2$(B) is a pseudocapacitive faradic process, rather different from the solid-state diffusion process observed for anatase [33]. The initial discharge capacity for the $TiO_2$(B)–SBR/CMC electrode is 258.5 mAh $g^{-1}$, which is slightly higher than that for $TiO_2$(B)–PVDF (249.3 mAh $g^{-1}$). Substantial irreversible capacity loss is observed in the first cycle for both electrodes. Such an irreversible capacity could be attributed to the inability to remove all the lithium ions that are inserted in the first discharge. Also, a part of irreversible capacity could be caused by the formation of SEI film which has been demonstrated recently by P. G. Bruce et al. [34]. As a result, the initial charge capacities for the $TiO_2$(B)–SBR/CMC and $TiO_2$(B)–PVDF electrodes are 232.1 and 226.9 mAh $g^{-1}$, with the corresponding Coulombic efficiency of 90% and 91%, respectively. Larger initial irreversible capacity loss was also observed in the literature for using CMC as binder compared with PVDF as binder [35,36]. This is probably related to the modification of the surface polymer layer on the SBR/CMC electrode that occurring in the first cycle.

Fig. 6b displays the cycling performance of different $TiO_2$(B) electrodes at the 0.2 C rate. The irreversible capacity loss for both electrodes is immediately minimized after the first cycle. A stable Coulombic efficiency of 99.8% is obtained for $TiO_2$(B)–SBR/CMC after six cycles, which is a little bit higher than that of $TiO_2$(B)–PVDF (99.5%). It is noticed that the Coulombic efficiency of $TiO_2$(B)–PVDF begins to vibrate after 40 cycles. This could be due to the poor electrode morphology (such as thick gel film, crack and stripping of the electrode film) as observed by SEM which causes instability of the battery performance. The $TiO_2$(B)–SBR/CMC electrode exhibits excellent capacity retention in that a high discharge capacity of 221 mAh $g^{-1}$ is obtained after 50 cycles. In contrast, the $TiO_2$(B)–PVDF electrode shows slow but continuous capacity decay, which only gives 196 mAh $g^{-1}$ after 50 cycles. This indicates that the binder plays an important role in the cycle stability of the $TiO_2$(B) electrode.

The rate capability and cycling performance of the $TiO_2$(B) electrodes prepared using different binders are performed from the 0.2 C ($I$ = 60 mA $g^{-1}$) to 15 C ($I$ = 4500 mA $g^{-1}$) rates as shown in Fig. 7a and b. Both the $TiO_2$(B)–PVDF and $TiO_2$(B)–SBR/CMC electrodes exhibit similar discharge capacities below the 1 C rate. The merit of SBR/CMC binder in the rate performance of the $TiO_2$(B) nanoribbons can be seen at higher rates. The discharge capacities of the $TiO_2$(B)–SBR/CMC electrode are 157.5 and 137.5 mAh $g^{-1}$ at the 2.5 C and 5 C rates, respectively. While smaller discharge capacities are obtained when using PVDF as binder, which are 146.6 and 119.7 mAh $g^{-1}$ correspondingly. Especially, only 45.9 and 15.9 mAh $g^{-1}$ are recorded for

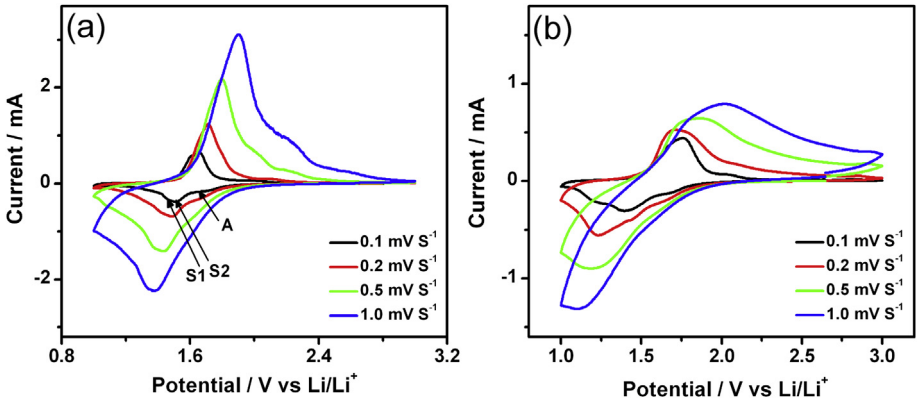


**Fig. 5.** CV curves of the $TiO_2$(B)–SBR/CMC (a) and $TiO_2$(B)–PVDF (b) electrodes at different scan rates from 0.1 to 1.0 mV $s^{-1}$ in the voltage window of 1.0–3.0 V.

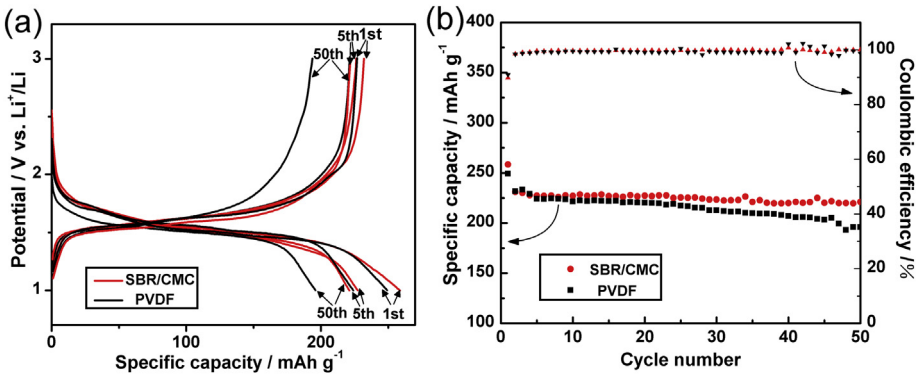


**Fig. 6.** (a) Charge–discharge curves (b) cycling performance and coulombic efficiency of the $TiO_2$(B)–SBR/CMC and $TiO_2$(B)–PVDF electrodes. All measurements are performed with the 0.2 C rate in the voltage window of 1.0–3.0 V.

$TiO_2$(B)–PVDF at the 10 C and 15 C rates, which are much smaller than those obtained for $TiO_2$(B)–SBR/CMC, i.e., 108.8 and 82.1 mAh $g^{-1}$, respectively. Fig. 7b and c compares the representative charge–discharge curves of the $TiO_2$(B)–PVDF and $TiO_2$(B)–SBR/CMC electrodes at different rates. Both electrodes show larger electrode polarization and IR drop with the increase of current rate. But this trend becomes more deteriorative for the $TiO_2$(B)–PVDF electrode. This indicates that the electrochemical kinetics of $TiO_2$(B)–PVDF are more sluggish than those of $TiO_2$(B)–SBR/CMC, resulting in its poor rate performance.

EIS is performed to study the electrochemical kinetics of the $TiO_2$(B)–SBR/CMC and $TiO_2$(B)–PVDF electrodes. The EIS measurement is first performed at the open circuit voltage (OCV). Then the electrode is charge–discharged for fifty cycles, followed by another EIS measurement at 3.0 V. Fig. 8 shows the Nyquist plots of different electrodes. The high-frequency intercept is attributed to the ohmic resistance which arises from the electrode, current collector and electrolyte et al. The ohmic resistance of $TiO_2$(B)–PVDF increases from 10.2 Ω to 17.5 Ω after fifty cycles, which can be attributed to the crack and striping of the electrode as indicated by the above SEM analysis. In contrast, the ohmic resistance of $TiO_2$(B)–SBR/CMC only slightly increases from 6.9 Ω to 7.63 Ω due to its excellent electrode maintainability. The semicircle at the OCV state is attributed to the interfacial impedance of the blocking electrode where no lithium ion insertion/extraction would proceed. At the OCV state, the interfacial resistance of $TiO_2$(B)–SBR/CMC is 29.5 Ω which is much smaller than that of $TiO_2$(B)–PVDF (198.9 Ω). This could be due to the use of SBR/CMC binder which can provide a more effective conductive network, high porous and uniform electrode morphology than the traditional PVDF binder. The charge

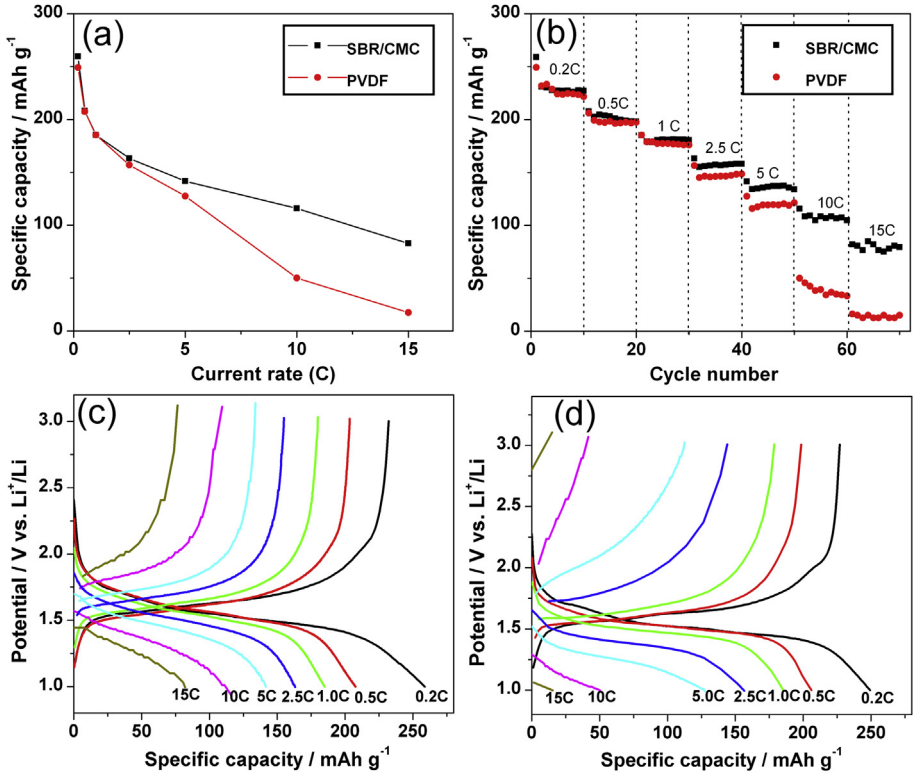


**Fig. 7.** (a) Rate capability (b) cycling performance and (c, d) charge–discharge curves of the $TiO_2$(B)–SBR/CMC and $TiO_2$(B)–PVDF electrodes.

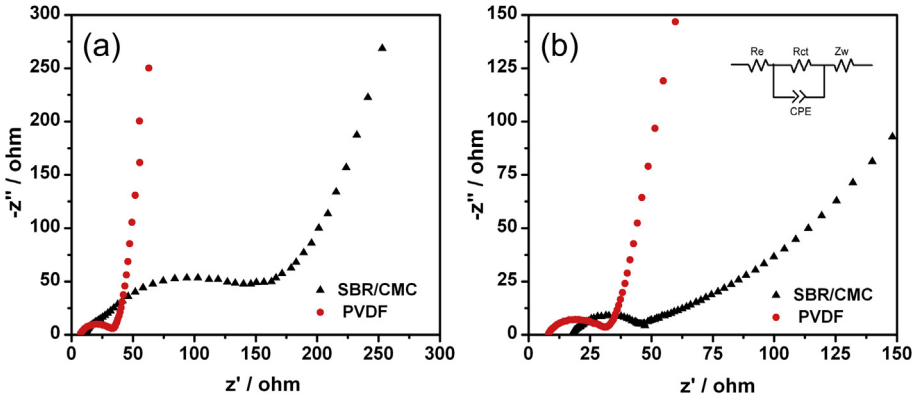


**Fig. 8.** Nyquist plots of the $TiO_2$(B)–SBR/CMC and $TiO_2$(B)–PVDF electrodes at the open circuit voltage (a) and after 50 cycles (b).

transfer resistance after fifty cycles is smaller than the interfacial resistance of the blocking electrode, which can be due to the activation of lithium ion insertion/extraction, deep soaking of the electrolyte, modification of the electrode/electrolyte interface et al. By simulating the Nyquist plots using the equivalent circuit in the inset of Fig. 8b, one can see that the charge transfer resistance of $TiO_2$(B)–SBR/CMC (24.8 Ω) is smaller than that of $TiO_2$(B)–PVDF (32.3 Ω). This indicates that the electrochemical kinetics of $TiO_2$(B)–SBR/CMC is better than that of $TiO_2$(B)–PVDF. As a result, the $TiO_2$(B) electrode prepared using the SMR/CMC binder shows better electrochemical performance than that prepared using the traditional PVDF binder.

### 3.4. Optimization of the $TiO_2$(B)–SBR/CMC electrode

In order to obtain superior performance, we further investigate the dependence of electrolyte on the electrochemical performance of the $TiO_2$(B)–SBR/CMC electrode. Currently the most widely used electrolyte in lithium-ion batteries is $LiPF_6$ which dissolved in ethylene carbonate (EC) and other co-solvents such as diethyl carbonate (DEC) and/or dimethyl carbonate (DMC). Here we study the rate performance of the $TiO_2$(B)–SBR/CMC electrode in different 1 M $LiPF_6$ electrolytes. As shown in Fig. 9, the rate performance decreases fast when using EC:DEC = 1:1 as the co-solvent. But it is greatly improved when replacing the DEC co-solvent by DMC. Especially, the electrolyte with more DMC (EC:DMC = 3:7) gives superior rate performance. The result is similar to that of the $TiO_2$(B)–PVDF electrode reported by Inaba et al. [37]. According to the authors, the superior rate performance can be attributed to the higher ionic conductivity and lower viscosity of the electrolyte due to the use more DMC co-solvent.

It is also important to study the dependence of electrochemical performance on the SBR/CMC binder contents to optimize the fabrication of the $TiO_2$(B) electrode. For this purpose, we prepared a series of $TiO_2$(B) electrodes using different SBR/CMC contents while keeping the super *P* content as 15 wt%. The electric resistance of the electrodes containing 18 wt%, 15 wt% and 12 wt% of SBR/CMC are 2.56 Ω, 2.03 Ω and 2.14 Ω, respectively. It shows that too much SBR/CMC content (18 wt%) results in larger electric resistance perhaps due to the high electric resistance of this organic binder. The electric resistance suddenly increases to 9.50 Ω when 9 wt% of SBR/CMC binder is used. Based on our experience, it is difficult to paste the electrode slurry onto the current collector using this small binder content, thus resulting in its larger electric resistance. Fig. 10 compares the rate performance of the $TiO_2$(B) electrodes with different SBR/CMC contents using the 1 M $LiPF_6$ electrolyte dissolved in EC:DMC = 3:7. The electrode with the smallest SBR/CMC content (9 wt%) exhibits the worst rate performance in all electrodes under investigation which can be due to its large electric resistance. The electrode with 18 wt% of SBR/CMC shows the largest capacities below the 2.5 C rate. However, the rate performance of

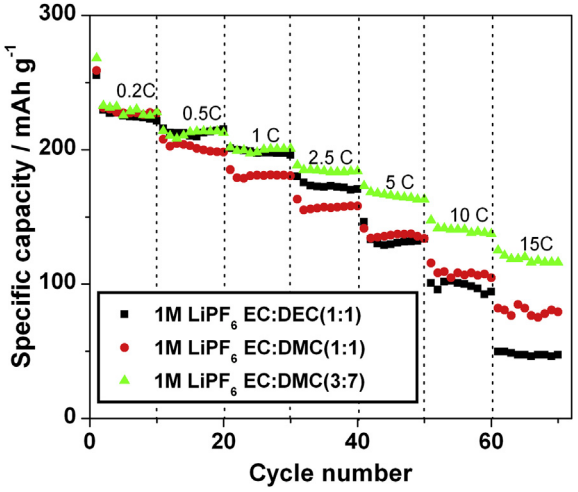


**Fig. 9.** Rate performance of the $TiO_2$(B)–SBR/CMC electrode in different $LiPF_6$-based electrolytes.

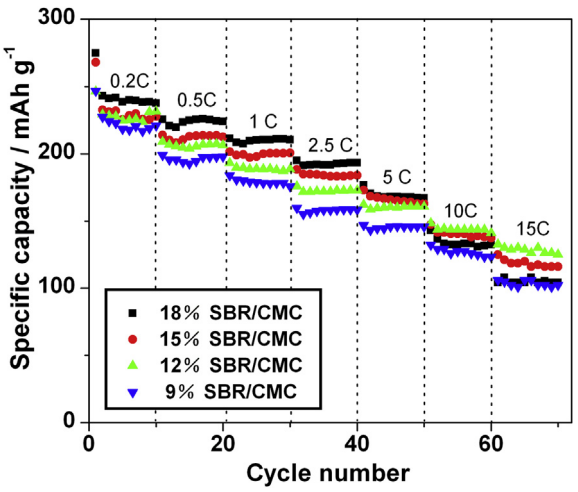


**Fig. 10.** Rate performance of the $TiO_2$(B) electrodes prepared with different SBR/CMC binder contents.

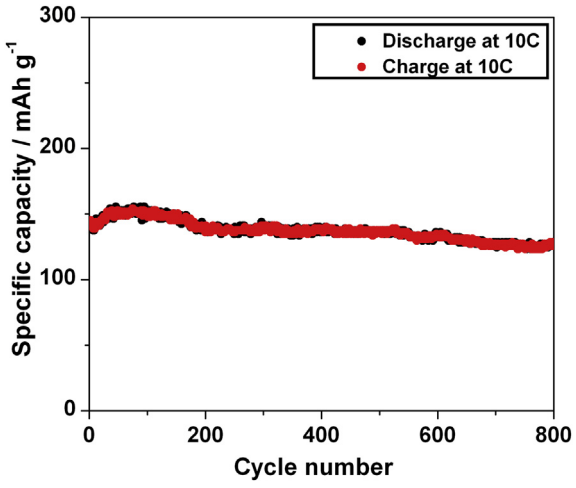


**Fig. 11.** Cycling performance of the $TiO_2$(B)–SBR/CMC electrode at the 10 C rate in the 1 M $LiPF_6$ electrolyte dissolved in EC:DMC = 3:7.

this electrode decreases fast at higher charge–discharge rates. In compromise, it is proposed that the optimized SBR/CMC binder content for the $TiO_2$(B) electrode is in the range of 12–15 wt%.

Based on the above analysis it is shown that the SBR/CMC binder is better than PVDF for the fabrication of $TiO_2$(B) electrode. The optimized SBR/CMC content is proposed to be in the range of 12–15 wt%. In addition, the 1 M $LiPF_6$ electrolyte dissolved in EC:DMC = 3:7 is more suitable for the $TiO_2$(B) electrode. Using this strategy we finally investigate the high rate performance of the $TiO_2$(B) electrode. As can be seen from Fig. 11, the discharge capacity of the electrode starts at 142.5 mAh $g^{-1}$ and still maintains at 127.6 mAh $g^{-1}$ after 800 cycles with a capacity loss of only 10.4%. The excellent long cycle life of the $TiO_2$(B)–SBR/CMC electrode demonstrates its promising applications in lithium-ion batteries especially for electric vehicles.

## 4. Conclusions

In summary, uniform one-dimensional $TiO_2$(B) nanoribbons are synthesized via the freeze-drying assisted hydrothermal method. The electrochemical performance of the $TiO_2$(B) electrodes prepared with the PVDF binder and the water SBR/CMC binder is investigated. The SBR/CMC binder is demonstrated to provide an effective three-dimensional network with uniform distribution of the $TiO_2$(B) active material and the super *P* conductive additive. In addition, the electrode exhibits very good maintainability during charge–discharge cycling which minimizes the gel deposition on the electrode, prevents the crack and striping of the electrode film. Due to these advantageous, the $TiO_2$(B) electrode prepared with the SBR/CMC binder exhibits higher specific capacities, better capacity retention and excellent high rate capability which are very attractive for lithium-ion batteries. In order to obtain superior electrochemical performance, the optimized SBR/CMC binder content for the $TiO_2$(B) electrode is proposed to be in the range of 12–15 wt%. We also suggest that the 1 M $LiPF_6$ electrolyte dissolved in the EC:DMC = 3:7 co-solvent is more suitable for the $TiO_2$(B)–SBR/CMC electrode which can provide excellent rate capability and capacity retention. This study demonstrates the possibility of manufacturing lithium-ion batteries using cheap aqueous binder, instead of expensive PVDF and hazardous organic solvents like NMP, thereby improving battery performance, reducing cost and protecting the environment.

## Acknowledgments

This work was supported by the 973 Program of China (no. 2009CB220104), the National Natural Science Foundation of China (no. 51272088), and the Research Fund for the Doctoral Program of Higher Education of China (no. 20110061130006).

## References

[1] D. Wang, D. Choi, J. Li, Z. Yang, Z. Nie, R. Kou, D. Hu, C. Wang, L.V. Saraf, J. Zhang, I.A. Aksay, J. Liu, ACS Nano 3 (2009) 907–914.
[2] J. Wang, J. Polleux, J. Lim, B. Dunn, J. Phys. Chem. C 111 (2007) 14925–14931.
[3] D. Deng, M.G. Kim, J.Y. Lee, J. Cho, Energy Environ. Sci. 2 (2009) 818–837.
[4] E. Baudrin, S. Cassaignon, M. Koesch, J.P. Jolivet, L. Dupont, J.M. Tarascon, Electrochem. Commun. 9 (2007) 337–342.
[5] Y.S. Hu, L. Kienle, Y.G. Guo, J. Maier, Adv. Mater. 18 (2006) 1421–1426.
[6] Z.X. Yang, G.D. Du, Z.P. Guo, X.B. Yu, Z.X. Chen, T.L. Guo, N. Sharma, H.K. Liu, Electrochem. Commun. 13 (2011) 46–49.
[7] H.S. Liu, Z.H. Bi, X.G. Sun, R.R. Unocic, M.P. Paranthaman, S. Dai, G.M. Brown, Adv. Mater. 23 (2011) 3450–3454.
[8] Q.J. Li, J.W. Zhang, B.B. Liu, M. Li, R. Liu, X.L. Li, H.L. Ma, S.D. Yu, L. Wang, Y.G. Zou, Z.P. Li, B. Zou, T. Cui, G.T. Zou, Inorg. Chem. 47 (2008) 9870–9873.
[9] M. Zukalová, M. Kalbáč, L. Kavan, I. Exnar, M. Graetzel, Chem. Mater. 17 (2005) 1248–1255.
[10] A.R. Armstrong, G. Armstrong, J. Canales, R. García, P.G. Bruce, Adv. Mater. 17 (2005) 862–865.
[11] A.R. Armstrong, G. Armstrong, J. Canales, P.G. Bruce, Angew. Chem. Int. Ed. 43 (2004) 2286–2288.
[12] R. van de Krol, A. Goossens, J. Schoonman, J. Phys. Chem. B 103 (1999) 7151–7159.
[13] S.-J. Bao, Q.-L. Bao, C.-M. Li, Z.-L. Dong, Electrochem. Commun. 9 (2007) 1233–1238.
[14] C. Jiang, I. Honma, T. Kudo, H. Zhou, Electrochem. Solid-State Lett. 10 (2007) A127–A129.
[15] P. Kubiak, M. Pfanzelt, J. Geserick, U. Hoermann, N. Huesing, U. Kaiser, M. Wohlfahrt-Mehrens, J. Power Sources 194 (2009) 1099–1104.
[16] P. Kubiaka, J. Geserick, N. Huesing, A. Wohfahrt-Mehrens, J. Power Sources 175 (2008) 510–516.
[17] J. Wang, Y. Bai, M. Wu, J. Yin, W.F. Zhang, J. Power Sources 191 (2009) 614–618.
[18] Y. Wang, M. Wu, W.F. Zhang, Electrochim. Acta 53 (2008) 7863–7868.
[19] A.R. Armstrong, C. Arrouvel, V. Gentili, S.C. Parker, M.S. Islam, P.G. Bruce, Chem. Mater. 22 (2010) 6426–6432.
[20] F.M. Courtel, S. Niketic, D. Duguay, Y. Abu-Lebdeh, I.J. Davidson, J. Power Sources 196 (2011) 2128–2134.
[21] J.H. Lee, U. Paik, V.A. Hackley, Y.M. Choi, J. Electrochem. Soc. 152 (2005) A1763–A1769.
[22] J. Li, H.M. Dahn, L.J. Krause, D.-B. Le, J.R. Dahn, J. Electrochem. Soc. 155 (2008) A812–A816.
[23] S.-L. Chou, J.-Z. Wang, C. Zhong, M.M. Rahman, H.-K. Liu, S.-X. Dou, Electrochim. Acta 54 (2009) 7519–7524.
[24] H. Buqa, M. Holzapfel, F. Krumeich, C. Veit, P. Novák, J. Power Sources 161 (2006) 617–622.
[25] B. Lestriez, S. Bahri, I. Sandu, L. Roué, D. Guyomard, Electrochem. Commun. 9 (2007) 2801–2806.
[26] M. Mancini, F. Nobili, R. Tossici, M. Wohlfahrt-Mehrens, R. Marassi, J. Power Sources 196 (2011) 9665–9671.
[27] M. Mancini, F. Nobili, R. Tossici, R. Marassi, Electrochim. Acta 85 (2012) 566–571.
[28] A. Moretti, G.-T. Kim, D. Bresser, K. Renger, E. Paillard, R. Marassi, M. Winter, S. Passerini, J. Power Sources 221 (2013) 419–426.
[29] D. Panduwinata, J.D. Gale, J. Mater. Chem. 19 (2009) 3931–3940.
[30] T. Beuvier, M. Richard-Plouet, L. Brohan, J. Phys. Chem. C 113 (2009) 13703–13706.
[31] J. Chong, S. Xun, H. Zheng, X. Song, G. Liu, P. Ridgway, J.Q. Wang, V.S. Battaglia, J. Power Sources 196 (2011) 7707–7714.
[32] H. Jang, S. Suzuki, M. Miyayama, J. Power Sources 203 (2012) 97–102.
[33] G.S. Zakharova, C. Jähne, A. Popa, C. Täschner, T. Gemming, A. Leonhardt, B. Büchner, R. Klingeler, J. Phys. Chem. C 116 (2012) 8714–8720.
[34] S. Brutti, V. Gentili, H. Menard, B. Scrosati, P.G. Bruce, Adv. Energy Mater. 2 (2012) 322–327.
[35] S.L. Chou, J.Z. Wang, H.K. Liu, S.X. Dou, J. Phys. Chem. C 115 (2011) 16220–16227.
[36] G.T. Kim, S.S. Jeong, M. Joost, E. Rocca, M. Winter, S. Passerini, A. Balducci, J. Power Sources 196 (2011) 2187–2194.
[37] M. Saito, Y. Murota, M. Takagi, M. Tajima, T. Asao, H. Inoue, A. Tasaka, M. Inaba, J. Electrochem. Soc. 159 (2012) A49–A54.